Modeling of Heat and Solute Interactions upon Grain Structure Solidification

Ch.-A. Gandin[1, a], J. Blaizot[1], S. Mosbah[1], M. Bellet[1],
G. Zimmermann[2, b], L. Sturz[2],
D. J. Browne[3, c], S. McFadden[3],
H. Jung[4], B. Billia[4, d], N. Mangelinck[4], H. Nguyen Thi[4],
Y. Fautrelle[5, e], X. Wang[5]

[1]MINES ParisTech, CEMEF, CNRS UMR 7635, Sophia Antipolis Cedex, France
[2] ACCESS e.V., Aachen, D
[3] University College Dublin (UCD), Dublin, IRL
[4] Université Paul Cézanne, Aix-Marseille III, Marseille, F
[5] EPM, INPG/ENSHMG, St Martin d'Hères, F

[a]Charles-Andre.GANDIN@mines-paristech.fr, [b]G.ZIMMERMANN@access.rwth-aachen.de,
[c]David.BROWNE@ucd.ie, [d]Bernard.BILLIA@im2np.fr, [e]Yves.FAUTRELLE@hmg.inpg.fr

Keywords: Solidification, Equiaxed, Columnar, Grain structure, Segregation, Modeling, Finite element, Cellular automaton.

Abstract

Simulations of several laboratory experiments developed for the study of structure and segregation in casting are presented. Interaction between the development of dendritic grain structure and segregation due to the transport of heat and mass by diffusion and convection is modeled using a Cellular Automaton - Finite Element model. The model includes a detailed treatment of diffusion of species in both the solid and liquid phases as presented elsewhere in this volume [1]. Applications deal with prediction of columnar and equiaxed grain structures, as well as inter-dendritic and inter-granular segregations induced by diffusion and macrosegregation induced by thermosolutal buoyancy forces.

Introduction

Structure in casting is closely related to segregation. While this is currently well understood and assessed at the microscopic scale using microsegregation models, it is much less tackled at the macroscopic scale of the cast ingots. Several sets of experimental data are now available that can be used to compare with model predictions. These data first come from directional solidification of Al-Si ingots, on ground and in microgravity, that exhibit classical columnar-to-equiaxed grain structure transitions. Experiments on solidification of SnPb alloys in a rectangular cavity are also available, for which both temperature maps and macrosegregation are measured. While several integrated modeling approaches have been developed, little comparison has yet been demonstrated with experimental observations. This contribution aims to present such comparisons using a two-dimensional (2D) Cellular Automaton (CA) – Finite Element (FE) model [1, 2, 3].

Upward directional solidification of Al-Si ingots

Upward directional solidification experiments of Al-Si cylindrical ingots with diameter 7 cm and height 18 cm were made available in the literature [4]. Thanks to the careful design of the experimental set-up and the casting procedure, the data could be used to compare with predictions of cooling curves and grain structures using several modeling approaches. For example, two types of one-dimensional (1D) models were developed. One was based on a 1D finite difference method

and a Landau transform to track the position of the boundaries of a columnar dendritic mushy zone [6] while the other was based on an averaging finite volume method [7]. Other models were developed to directly compute the grain structure, for example, the coupled Cellular Automaton (CA) - Finite Element (FE) method [5] and the two-dimensional (2D) front tracking method [8], where each grain was seen as a portion of the mushy zone developing in the ingot as a result of the nucleation and growth of dendritic grains. All these models account for the undercooling of the dendritic mushy zone and converge towards the conclusion that, in these Al-Si experiments, fragmentation of the columnar growth front could be the mechanism to explain the origin of the equiaxed grains and the Columnar-to-Equiaxed Transition (CET) observed in the ingots. This finding was deduced from the fact that nucleation undercooling of the equiaxed structure needed to be set equal to the growth undercooling of the columnar dendritic front in order to simulate the position of the CET. This position also corresponded to the maximum undercooling the columnar dendritic front would reach if no equiaxed grains nucleated. Indeed, a decrease of the growth velocity of a columnar front is known in the literature as bringing about the onset of fragmentation due to secondary dendrite arm remelting [9]. Fragmentation is also a phenomenon that has been observed in Al-Si and Al-Cu alloys using in situ and in real time X-Ray imaging [12, 13].

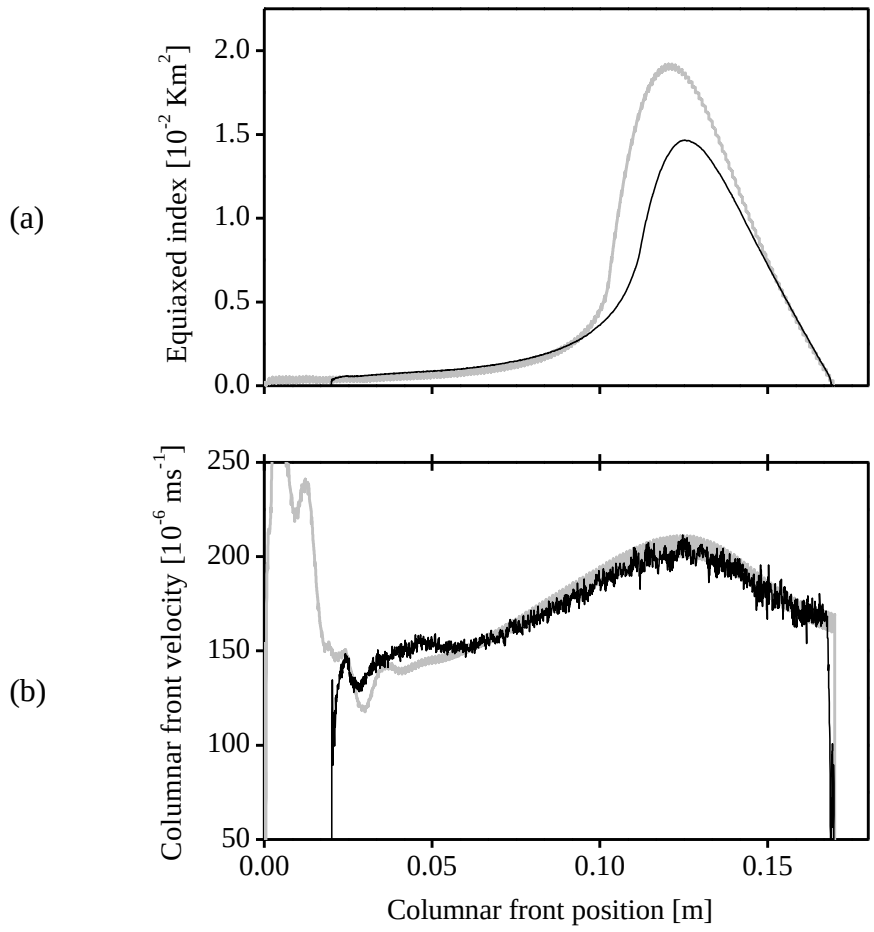

Figure 1. Predicted evolution of (a) the equiaxed index [10] and (b) the columnar growth front velocity upon solidification of an Al-7wt%Si ingot [6] using (grey lines) a 2D front tracking model [11] and (black lines) the CAFE model [1].

Recently, a CET criterion based on the maximum value reached by an equiaxed index has been proposed [10]. The index is calculated by integrating over the simulation domain the local undercooling of the melt. If divided by the total volume of the undercooled melt, this index would thus be very similar to calculating an average undercooling of the melt. Figure 1a presents the evolution of the equiaxed index predicted as a function of the position of the mushy zone growth front during its upward propagation into the melt. It compares prediction of the 2D front tracking model (grey line) [11] with the coupled CAFE model (black line). As can be seen, very similar results were obtained. Variations are due to the differences between the modeling approaches, the boundary condition used to treat the heat transfer between the alloy and the chill located at the bottom of the domain, and the numerical implementation of the growth kinetics model for the dendrite tips [14]. By comparing Figures 1a and 1b one can easily see that the maximum of the equiaxed index indeed corresponds to the maximum velocity reached by the columnar growth front. It is located about 12 cm from the bottom of the ingot, i.e. at the position measured for the CET. The reason was well explained by a simple 1D heat flow analysis [6]. Upon extraction of the superheat from the melt, the columnar growth front velocity first increased. The subsequent decrease of the velocity corresponded to the absence of melt superheat, i.e., there was no remaining temperature gradient in the liquid ahead of the columnar growth front, while the temperature gradient in the mushy zone behind the columnar growth front naturally decreased due to the increasing distance from the chill. Application of the equiaxed index criterion to other Al-Si alloys is available elsewhere [11]. This explanation for the CET will be retrieved in the next section.

μg and 1g directional solidification of Al-7wt%Si rods

Solidification experiments have recently been carried out in 200 mm long and 8 mm diameter Al-7wt%Si rods under terrestrial and reduced gravity conditions. Details of the set-up are presented by Sturz and Zimmermann [15, 16]. The reduced gravity conditions were accessible thanks to the MAXUS-7 sounding rocket. The system is shown schematically in Figure 2 with a 2D cylindrical coordinate approximation. The contours of the five simulation domains are drawn using plain black lines. The Al-7wt%Si alloy is located on the left-hand-side, maintained by a steel block at the bottom and a boron nitride (BN) plug at the top. The crucible is made of an inner alumina tube (Al_2O_3) inserted into an outer nickel (Ni) tube. Cooling histories are measured using eight NiCrNi thermocouples located in the Al_2O_3 crucible at about 0.5 mm from the alloy/crucible interface. The locations of the thermocouples, T_1 to T_8, are marked in Figure 2 with cross symbols. These demarcations correspond to the following distances from the bottom of the Al-7wt%Si rods: T_1: 83 mm, T_2: 103 mm, T_3: 113 mm, T_4: 123 mm, T_5: 133 mm, T_6: 143 mm, T_7: 153 mm and T_8: 163 mm. Three zones of controlled temperatures (hereafter called "heaters" and labeled H_1 to H_3 in Figure 2) are used to control heating and cooling of the system. In the experiment, this was achieved by using feedback control on the temperatures recorded by the closest thermocouples to the heaters. The temperatures at the thermocouples could be changed by heating or letting it be cooled down.

The geometry of the heaters was not directly modeled. Instead, the recorded temperature history of thermocouples T_1, T_5 and T_8 were imposed using Dirichlet boundary conditions at the three zones labeled H_1 to H_3 in Figure 2. The experimental procedure to reach the initial steady temperature profile is explained in details elsewhere [15, 16]. In the calculations, the initial steady temperature profile could be modeled by simply imposing an initial 700 °C temperature to the five simulation domains and let the system equilibrate for 200 s to the temperatures imposed to the heaters. As can be read from the temperature history in Figure 2, the simulated temperature profile reaches the measured profile at the onset of cooling, i.e. when the solidification experiment started.

The cooling curves in Figure 2 reveal an almost perfect match between the measured and simulated cooling curves. This is due to the Dirichlet boundary conditions imposed in the

simulation using experimental measurements as well as well knowing thermal properties for the Al-7wt%Si alloy [6]. The time evolution of the temperature profile drawn from the cooling curves extracted from the calculations at the location of the thermocouples consequently compares favorably with the experimental results as shown in Figure 2b. From the simulation it was possible to draw the time evolution of the temperature profiles on the axis of symmetry of the simulation domains, i.e., in the alloy, as well as in the crucible where the thermocouples are located. This is shown in Figure 3a where the plain black curves and the dashed grey curves correspond to profiles in the alloy and in the crucible, respectively.

Figure 3a reveals more precisely the dynamics of the heat flow upon the occurrence of the CET when using narrower ranges for the temperature and a shorter time interval. The corresponding time sequence of the development of the grain structure is made available in Figure 3b at three successive times, as well as at the end of the simulation. It can be seen that the cooling rate drastically increased in the liquid when little superheat remained. Indeed, at time 795 s, the columnar front was fully developed with no possibility for the equiaxed grains to nucleate and grow. The reason for this is that the liquid was not sufficiently undercooled ahead of the growth front in order to allow equiaxed nucleation. Note that the temperature profile at time 795 s reveals that the growth front was located at position 150 mm and its temperature was slightly lower than 614 °C, thus corresponding to more than 4° C of undercooling. At this time the temperature of most of the liquid was above the liquidus of the alloy, i.e. 618 °C. Just a few seconds later, the entire remaining liquid domain was fully undercooled as shown by the profile drawn at 615 s. Note that the heat flux between the alloy and the plug lead to some undercooling at the right-hand-side of the ingot. A calculation with an adiabatic condition between these two domains would have left to the same global temperature profile, i.e. a fully undercooled liquid. Nucleation remained limited ahead of the advancing columnar front as shown by grain structure at time 615 s. These newly-nucleated grains were able to stop the growth of the columnar front but developed in a rather elongated shape, which is in agreement with the observation of a limited mixed zone as observed in the experimental cross section through the sample displayed in Figure 3c. Finally, at time 635 s, the equiaxed grain structure fully developed thanks to a further decrease of the temperature of the melt at that time. As a consequence of the heat released outside the envelope of the grains, the temperature in the alloy becomes higher than in the crucible at time 635 s. This is opposite to what was observed at previous times.

A good comparison with the measured position of the CET was retrieved when comparing Figure 3b and c. This was possible thanks to the adjustment of the nucleation parameters of the CA model. A Gaussian distribution of the density of the nucleation site was used as a function of the liquid undercooling, with parameters a mean undercooling (5.2 K), a standard deviation (0.5 K) and a total density (10^9 m^{-3}) [5]. Adjusted nucleation distribution values lead to nucleation of equiaxed grains at an undercooling very close to the growth undercooling of the columnar front when no temperature gradient remained in the liquid. This observation was in full agreement with results and interpretations previously reported for the CET in non-inoculated Al-7wt%Si alloys [6-8].

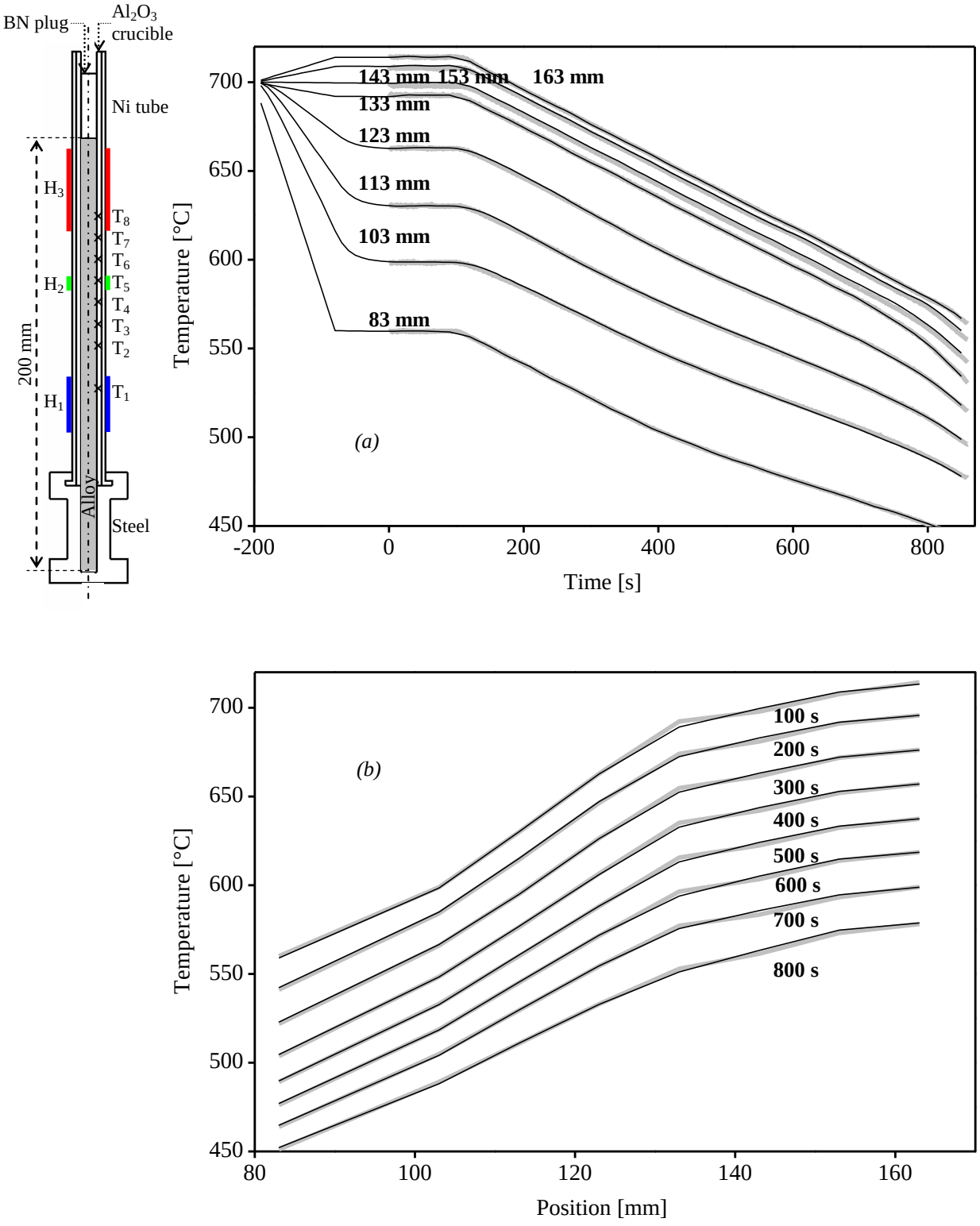

Figure 2. Temperature (grey) measured and (black) predicted during the microgravity directional solidification experiment of an Al-7wt%Si rod (a) as a function of time at the location of the thermocouples, (b) as a function of the position for at 8 successive times during the experiment. The black lines of the drawing on the left-hand-side are made from the contour of the 5 simulation domains used to compute the heat flow using the CAFE model with cylindrical coordinate approximation. The axis of symmetry of the cylindrical coordinates system is displayed at the center of the rod. Locations of the heater (H_1-H_3) and thermocouples (T_1-T_8) are also indicated.

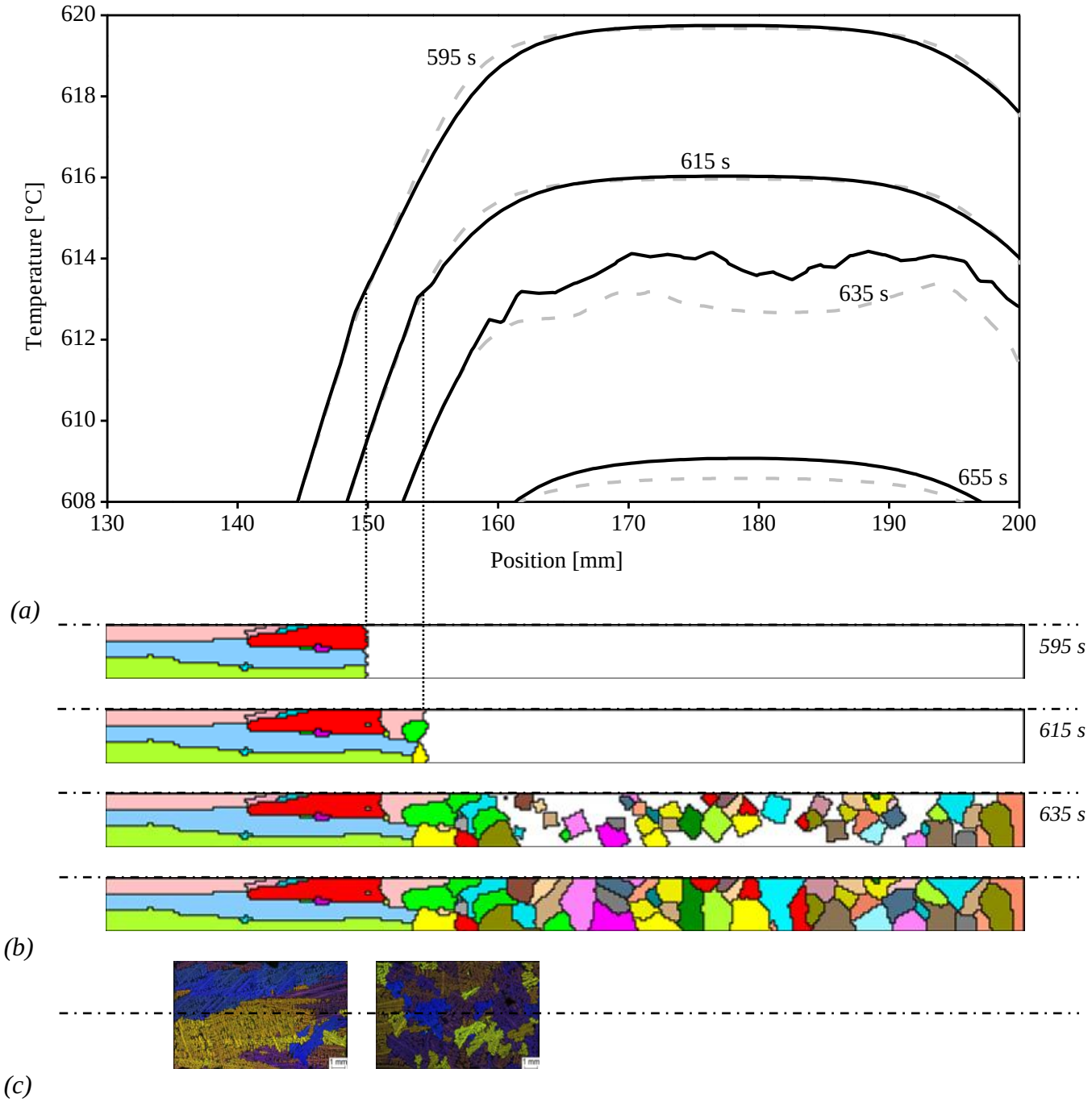

Figure 3. Time sequence of (a) temperature profiles (plain balck curves: alloy, dashed gray curves: crucible), (b) grain structures simulated with the axisymmetrical 2D CAFE model and (c) as-cast structure observed in the retrieved microgravity samples (range of observation: 134.8 mm and (right) 163.9 mm.

Sn-Pb rectangular casting

An experimental set-up has been designed for the study of macrosegregation induced by thermosolutal buoyancy forces. It is heavily inspired from the previous work proposed by Hebditch and Hunt [17]. Parallelepiped geometry is used with dimensions 10×6×1 cm^3. It is filled with a Sn-10wt%Pb alloy. The smallest surfaces of the casting, i.e. the two opposite faces with dimension 6×1 cm^2, are in contact with temperature controlled heat exchangers. Their temperature evolutions are thus imposed with time using either constant heating/cooling rates or holding temperatures. All other surfaces are made adiabatic as explained in details in [18].

The experimental procedure is the following. The ingot is first melted and maintained in a liquid state during sufficient time for temperature homogenization at 250 °C, which can be checked by reading the array of thermocouples. A temperature gradient of 200 K m^{-1} is then imposed through the liquid by prescribing a heating rate and a temperature plateau at 270 °C with the right-hand-side heat exchanger. After a holding period, an identical cooling rate of 0.03 K s^{-1} is imposed on both heat exchangers while maintaining the initial 20 K temperature difference between the smallest faces of the parallelepiped geometry, thus leading to solidification of the alloy.

An array of 50 thermocouples is used to record the temperature during the experiment. It consists of 5 rows with 10 thermocouples, each thermocouple being distant from its neighbour by 1 cm in both the vertical and horizontal directions. This grid of thermocouples is used to measure the evolution of experimental temperature maps at the surface of one of the 10×6 cm^2 faces as shown in the time sequence of Figure 4. Careful analyses of the flow within the thickness of the ingot (1 cm) shows almost no temperature gradient in the transverse direction. Due to the small value of the Biot number, the temperature could be assumed uniform in the thickness. This could be checked using a 3D simulation of the heat flow.

In addition to the in-situ measurement of the temperature maps, the average composition of Pb has been measured in the as-solidified sample using the same grid. The 50 values collected are then used to draw the final average Pb composition as shown in Figure 5. Figure 6 gives a picture of the as-cast grain structure as observed at the surface of the ingot. Again, comparison with the grain structure on the opposite large face of the ingot reveals minor differences.

A 2D Cartesian CAFE simulation has been performed using the parameters shown in Table 1. As can be seen good agreement is achieved for the time sequence of the temperature maps (Figure 4) and the average segregation map (Figure 5). Unlike previous simulations presented in this contribution, macrosegregation is mainly due to thermosolutal convection. Upon solidification, the liquid is enriched with Pb and generate a buoyancy force caused by the density variation with composition. Note that the calculation still considers diffusion in both the solid and liquid phases and thermal convection, although these effects are not the main mechanisms to explain the final macrosegregation. Similarities exist with the simulated macrosegregation in other SnPb alloys [2] and GaIn alloys [3] also using rectangular castings. Unlike for previous AlSi alloys, properties are not well known for SnPb alloys. In particular one can note in Table 1 that the thermal expansion coefficient has been adjusted to a rather small value. This was done by comparing the calculated temperature maps with the measurements prior to the start of solidification, i.e. when only thermal convection takes place. It is not yet clear whether this is justified since little measurement data exist for this coefficient. One reason to use this small value could also be due to layering of Pb in the liquid state formed upon melting of the alloy, which would stabilize the thermal convection.

Figure 6 presents the simulated grain structure. The grains appear much coarser than the experimental grain structure. The main reason for this difference is believed to be due to the absence of grain sedimentation. In the simulated grains structure, after nucleation in the undercooled liquid, grains remain fixed in space and can only grow. This was already shown in the past as a main limitation if one wishes to compare together grain structure and segregation [2]. An interesting feature is the growth of the grains that are connected to the bottom part of the ingot. These grains were not nucleated at the mould wall but grew from the inside of the casting toward the mold wall. The reason is easily understood when considering the average composition map shown in Figure 5. A large zone enriched in Pb forms at the bottom part of the ingot, which reproduces well the experimental measurement. Upon solidification, this zone is the last to solidify because it requires decreasing the temperature below the local liquidus temperature. Consequently, the existing grains do grow in this pocket of liquid from the inside of the ingot toward its bottom edge, explaining the elongated shape of the grains.

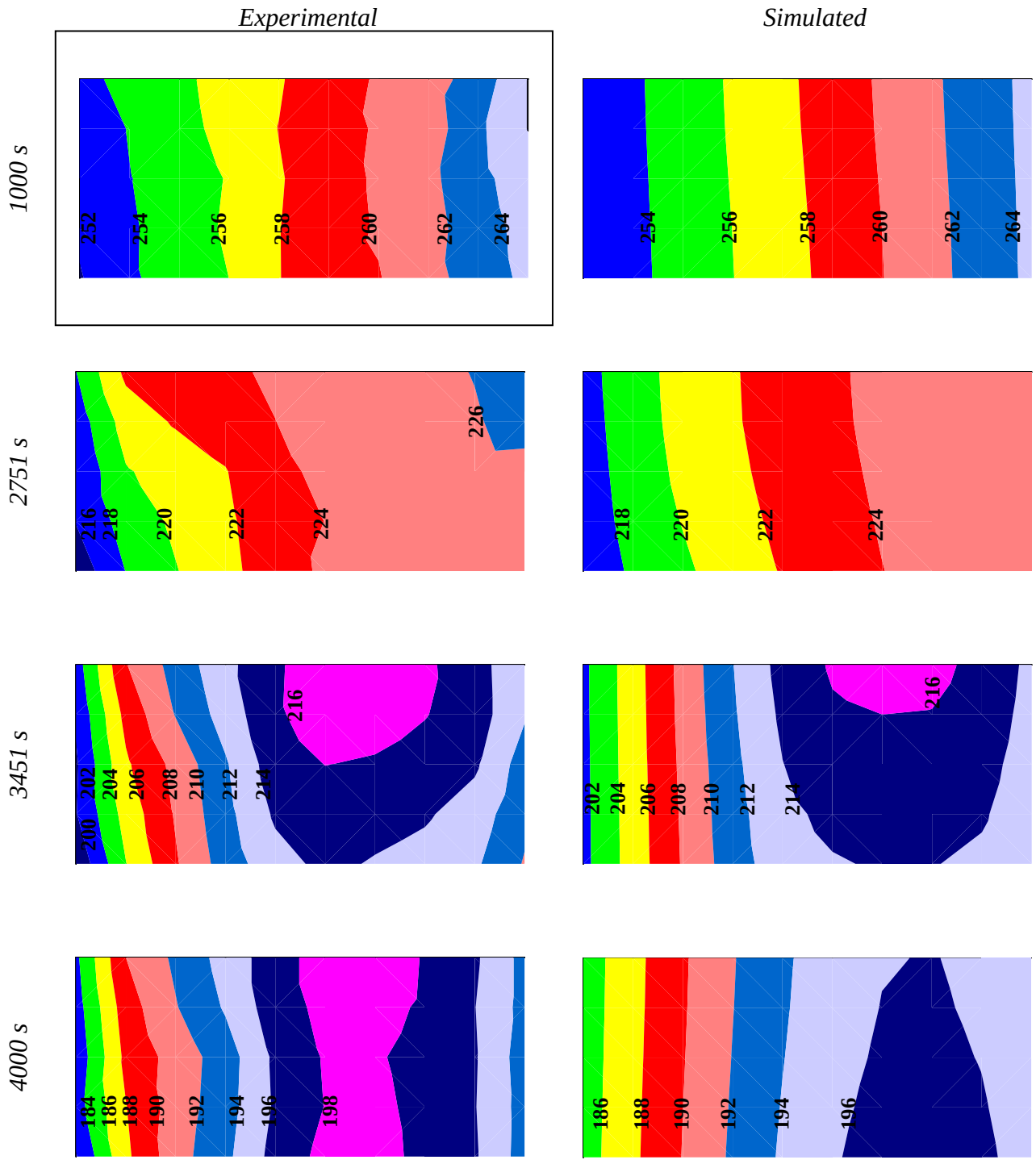

Figure 4. (left) measured and (right) simulated temperature maps at different time during the experiment of a Sn-10wt%Pb alloy. The black rectangle in the top-left figure indicates the representative size of the 10×6 cm^2 ingot.

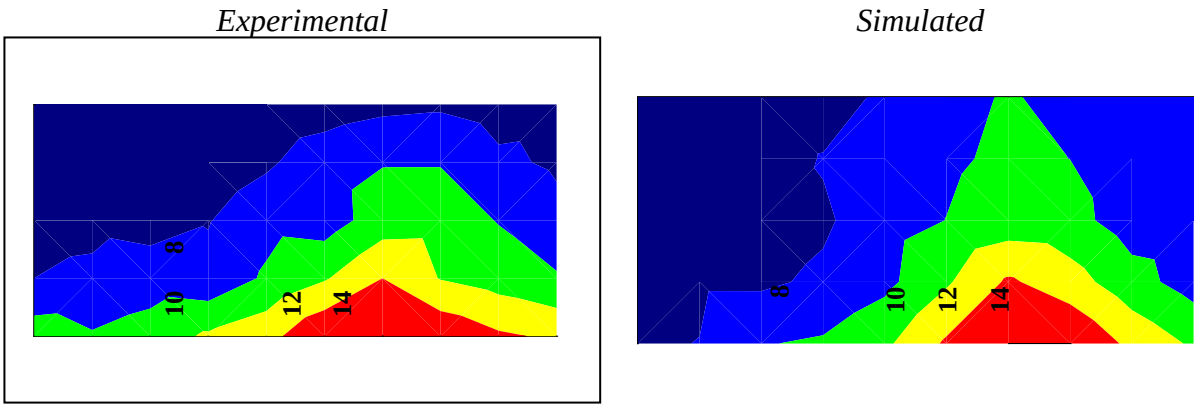

Figure 5. Average wt% Pb composition of a Sn-10wt%Pb (left) measured and (right) simulated. The black rectangle in the left figure indicates the representative size of the 10×6 cm^2 ingot.

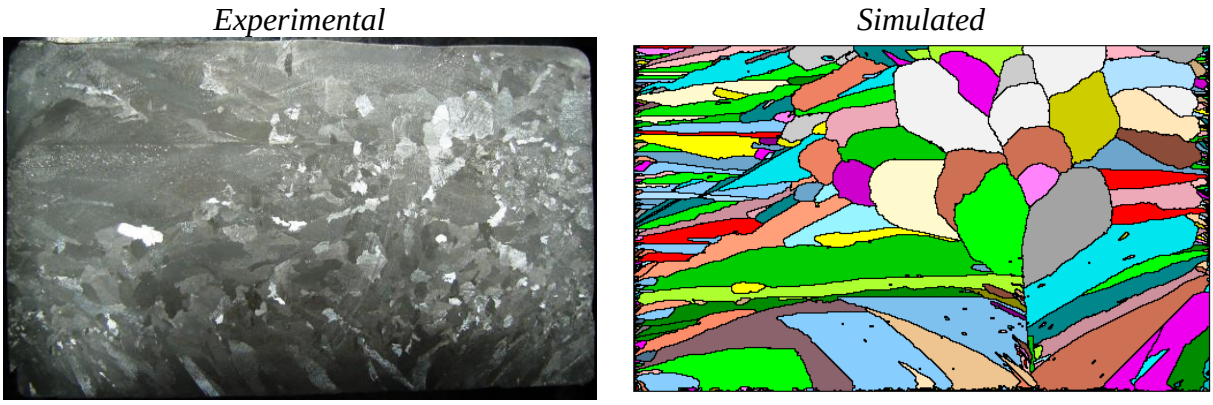

Figure 6. Solidification grain structure of a Sn-10wt%Pb (left) as observed at the surface of the casting and (right) simulated. Ingot size: 10×6 cm^2.

Latent heat of fusion	J kg^{-1}	3 10^4	Initial temperature	°C	249
Heat capacity	J kg^{-1} $°C^{-1}$	260	heat exchangers cooling rate	°C s^{-1}	-0.03
Thermal conductivity in solid	W m^{-1} $°C^{-1}$	50	Time step	s	0.5
Thermal conductivity in liquid	W m^{-1} $°C^{-1}$	20	Temperature difference between left-		
Melting temperature	°C	232	and right-hand-side heat exchangers	°C m^{-1}	20
Eutectic temperature	°C	183			
Liquidus slope	°C $wt\%^{-1}$	-1.294	*Additional parameters for a CAFE simulation*		
Segregation coefficient	-	0.09	Diffusion coeff. (Pb in liquid Sn)	m^2 s^{-1}	4.5 10^{-9}
Eutectic composition	wt%	37.87	Diffusion coeff. (Pb in solid Sn)	m^2 s^{-1}	5 10^{-13}
Liquid density	kg m^{-3}	7371	Gibbs-Thomson coefficient	K m	5.68 10^{-8}
Nominal Pb composition	wt%	10	Nucleation undercooling		
Thermal expansion coefficient	$°C^{-1}$	8 10^{-9}	Mean	°C	1.2
Solute expansion coefficient	$wt\%^{-1}$	-5 10^{-3}	Standard deviation	°C	0.2
Dynamic viscosity	Pa s	10^{-3}	Total density	m^{-3}	5 10^8
Dendrite arm spacing	m	100 10^{-6}	Cell size	m	2 10^{-4}

Table 1: Value of the material properties of the Sn-Pb rectangular casting simulations.

Summary

The present article has demonstrated the possibility to use the 2D CAFE model for a systematic study of grain structure and segregation formed in casting. This is possible thanks to the new developments of the model that include diffusion in both the solid and liquid phases, as well as a remeshing technique to track the development of mushy zone - liquid boundaries, i.e. the grain envelopes [1]. Further developments are yet required in order to get access to a more realistic description of the grain structure. This includes the need to further develop a three-dimensional version, as well as to implement efficient treatments of the transport of the grains.

Acknowledgments

This work was conducted within a European Space Agency project of the Microgravity Applications Promotion program (project "COLUMNAR-TO-EQUIAXED TRANSITION IN SOLIDIFICATION PROCESSING (CETSOL)", contract 14313/01/NL/SH). The 2D CAFE model is developed in the software R2Sol-CA.

References

[1] Mosbah S., Bellet M., Gandin Ch.-A. This proceeding.

[2] Guillemot G., Gandin Ch.-A., Combeau H., ISIJ International 46 (2006) 880.

[3] Guillemot G., Gandin Ch. -A., Bellet M. Journal of Crystal Growth 303 (2007) 58.

[4] Gandin Ch.-A. ISIJ int. 40 (2000) 971.

[5] Gandin Ch.-A., Rappaz M. Acta metall. 42 (1994) 2233.

[6] Gandin Ch.-A. Acta mater. 48 (2000) 2483.

[7] Martorano M.A., Beckermann C., Gandin Ch.-A. Metall. mater. trans. 34A (2003) 1657.

[8] McFadden S., Browne D.J. Appl. math. model. In press. doi:10.1016/j.apm.2008.01.027.

[9] Jackson K. A., Hunt J. D., Uhlmann D. R., Seward III T. P. Trans. AIME 236 (1966) 149.

[10] Browne, D.J. ISIJ int. 45 (2005) 37.

[11] McFadden S., Browne, D.J., Gandin Ch.-A. Metall. mater. trans. A. In press.

[12] Jung H., Mangelinck-Noël N., Nguyen-Thi H., Bergeon N., Billia B., Buffet A., Reinhart G., Schenk T., Baruchel J. International Journal of Cast Metal Research (2008). In press.

[13] Ruvalcaba D., Mathiesen R.H., Eskin D.G., Arnberg L., Katgerman L. Acta Materialia 55 (2007) 4287.

[14] Gandin Ch.-A., Guillemot G., Appolaire B., Niane N. T. Mater. Sci. Engng A342 (2003) 44.

[15] Sturz L., Zimmermann G., International Journal of Cast metals Research 20 (2007) 122.

[16] Sturz L., Zimmermann G., Jung H., Mangelinck-Noël N., Nguyen-Thi H., Billia B. 18th ESA Symposium on European Rocket and Balloon Programmes and Related Research. Ed. by L. Conroy, ESA SP 647, Communication Production Office, Nordwijk, NL (2007) 367.

[17] Hebditch D. J. , Hunt J. D. , Metall. Trans. 5 (1974) 1557.

[18] Wang X. D., Petitpas P., Garnier C., Paulin J. P., Fautrelle Y., in Modeling of Casting, Welding and Advanced Solidification Processes XI, TMS, Warrendale, PA, USA (2006).